Chapter 4

Periodically Driven Hard Core Bosonic Systems

4.1 Introduction

Hard core bosons (HCBs) are normal bosons, but they strongly interact with each other in a repulsive manner. The strong repulsion prevents two bosons from being at the same point in position/lattice space. This behavior of the HCBs is qualitatively similar to the spinless fermions, which also do not occupy the same point in position space due to the well known Pauli's exclusion principle. Therefore, at the same position/lattice point, the HCBs behave like spinless fermions; but when two HCBs are found in two different places, then their exchange property follows the commutation rule of the standard bosons. However, though the physical reasons behind the absence of more than one HCBs and spinless fermions at the same point on space are different, still the HCBs can simulate many properties of the spinless fermions. Particularly, many of the well known theories of solid state physics, related to the spinless fermions, can be simulated by the HCBs. This relation or mapping between the HCBs and the spinless fermions is established theoretically by

the celebrated Jordan-Wigner (JW) transformation. The HCBs have already been realized experimentally in cold atoms on optical lattice [99, 100]. This has opened a new avenue where different solid state systems can be simulated experimentally by the cold atoms on the optical lattice setup.

The idea of the HCBs was proposed a long time back by Tonks, and later the idea was extended by Girardeau. Thus this bosonic gas is known in the literature as the Tonks-Girardeau (TG) gas [101, 102]. In this original idea, this strongly interacting bosonic gas was assumed to move on continuous space. In more recent times, this gas was studied extensively on the periodic lattice, and it has got another name hard core bosons.

Recently, the HCBs are studied on a 1D lattice with a periodically driven onsite staggered potential. The onsite staggered potential introduces a gap in the energy band of the HCB system, which is otherwise a gapless system having superfluid property. The system makes a quantum phase transition due to the gap formation in the spectrum by the staggered potential and becomes a bosonic Mott insulator. For the periodically driven staggered potential cases, the phase transition happens periodically in time. In case of the sinusoidal driving, the opening and closing of the gap also happens sinusoidally and so the phase transition [39]. The same system is studied for another driving protocol of the form of δ-function kicks [40]. The HCB lattice experiences a single δ-kick within a time period T. This system shows dynamical localization (DL), which is manifested in the decay of the initial current flow through the system. The DL is a well known property that is observed in many dynamical systems, particularly in nonintegrable or chaotic systems: for example, Kapitza pendulum [32], quantum kicked rotors [31, 79], driven two-level systems [28], etc. The δ-kicked HCB 1D lattice is now another system which shows the DL.

We have witnessed in Chapter 3 that, instead of a single δ-kick, double δ-kicks can drastically alter the dynamics as well as the spectrum of a system. Therefore, we are now going to study the HCB system experiencing two δ-kicks within a single time period. Like the double kicked top system, here we have again considered the polarity or the direction of the second kick opposite to the first kick. Therefore, the second kick gives us the freedom to tune the first kick's effect by varying the driving strength and the time separation between the two kicks. We have found that the second δ-kick driving can remove the observed DL in the single kicked case partially or completely.

The periodic driving on the HCB system prompted us to study this system from the Floquet theory perspective. As we know that the derivation of the effective Hamiltonian is generally possible by only some perturbation techniques. Since the HCB system in the presence of onsite staggered potential is a two-bands system; then in the momentum basis, one can represent the Hamiltonian in a 2×2 matrix form using the Pauli matrices. Therefore, for the δ-kicked cases, instead of employing any perturbation theory, one can always derive the effective Hamiltonian of the HCB system exactly by analytical means. This is one of the major reasons for us to study this model of HCB system under the Floquet theory.

We introduce the HCB model and discuss the formalism for the derivation of the effective Hamiltonian from the Floquet operator in Sec. 4.2. Here we also define two local observables which we have studied extensively: the current operator and the work done on the system. In Secs. 4.3 and 4.4, we respectively study the single and double δ-kicked HCB system. Since the single kicked HCB system has been studied earlier [40], here we have studied some of its basic features but from our formalism. The double kicked system is studied very elaborately as a function of all system parameters. Besides the current flow and the work done on the system,

we have also studied how the density of particles evolve in time. We have then drawn a phase diagram of the system on a pair of parameters space, and have identified the regions with superfluid, Mott insulator and the intermediate of the two. Finally, we conclude in Sec. 4.5.

4.2 The Model: driving protocols, observables, initial state, and dynamics

We now introduce the model of HCB. Moreover, we discuss the driving protocols, the observables which we have calculated, the initial state of the system, and the time evolution (dynamics) of the observables. We have extensively studied two observables: particle current flow through the system and the work done on the system by the periodic driving. Here, we consider two different driving protocols: single and double kicks. For both the protocols, we consider the same initial state. Finally, we describe a general theory of the dynamical evolution of the observables.

4.2.1 Model

We have considered a chain of hard core bosons (HCBs) on a 1D lattice for the half-filling case. The corresponding Hamiltonian at the tight binding limit can be written as

$$H = -\gamma \sum_{l=1}^{L} \left(b_l^\dagger \, b_{l+1} \, + \, b_{l+1}^\dagger \, b_l \right), \tag{4.1}$$

where $b_l^\dagger$ and b_l are the bosonic creation and annihilation operators, respectively. The creation operator $b_l^\dagger$ increases the number of bosons at site l by *one*; whereas the annihilation operator b_l decreases the number of bosons by *one* at the same site l. The bosonic operators satisfy the commutation relation, $[b_l, b_{l'}^\dagger] = 0$, and the hard core relation $b_l^2 = b_l^{\dagger 2} = 0$. The hard core relation ensures the presence of

at the most one boson per lattice site. The parameter γ is defined as the hopping amplitude between two neighboring sites and assumed to be positive. We set $\gamma = 1.0$, which suggests that all the other parameters are measured in the unit of the hopping amplitude γ. Using Jordan-Wigner (JW) transformation, the HCBs can be mapped in to the noninteracting spinless fermions [103]. This transformation is possible due to the following reason: fundamentally the HCBs are normal bosons. However, they interact infinitely strong repulsive manner, which do not allow them to stay at the same site. Therefore, in the real space or the lattice space, their behavior qualitatively similar to the normal fermions. However, the fermions do not stay at the same site because of the Pauli's exclusion principle. Even though the different physical reasons, the HCBs at some extend mimics the property of the fermions. Therefore, the HCB model can simulate many of the theories of solid state physics for the spinless Fermions. Here, for the sake of completeness, we have shown how the JW transformation maps the HCB Hamiltonian to the fermionic Hamiltonian. The JW transformation is defined as:

$$f_l = \exp\left[i\pi \sum_{l'=1}^{l-1} b_{l'}^\dagger\, b_{l'}\right] b_l \qquad \text{and} \qquad f_l^\dagger = b_l^\dagger\, \exp\left[-i\pi \sum_{l'=1}^{l-1} b_{l'}^\dagger\, b_{l'}\right], \tag{4.2}$$

where $f_l^\dagger$ and f_l are the fermionic creation and annihilation operator, respectively. Here we have considered the periodic boundary condition. Therefore, the Hamiltonian has one hopping term at the *boundary* as $b_L^\dagger b_1$ and its Hermitian conjugate. Therefore, the HCB hamiltonian, given in Eq. (4.1), can explicitly be written as

$$H = -\left[\sum_{l=1}^{L-1}\left(b_l^\dagger\, b_{l+1} + b_{l+1}^\dagger\, b_l\right) + \left(b_L^\dagger b_1 + b_1^\dagger b_L\right)\right]. \tag{4.3}$$

Then, via JW transformation, the Hamiltonian in terms of the fermionic operators becomes

$$H = -\left[\sum_{l=1}^{L-1} f_l^\dagger f_{l+1} + \text{h.c.}\right] - \left[f_L^\dagger f_1 \exp\left(i\pi \sum_{l'=1}^{L-1} f_{l'}^\dagger f_{l'}\right) + \text{h.c.}\right], \tag{4.4}$$

here we consider $f_l^{\dagger^2} = f_l^2 = 0$. The operator $f_{l'}^\dagger f_{l'}$ is the occupation number, having value either 0 or 1. Consequently, $\sum_{l'=1}^{L-1} f_{l'}^\dagger f_{l'}$ is the total number of particles which can either be odd or even integer. Therefore, $\exp\left(i\pi \sum_{l'=1}^{L-1} f_{l'}^\dagger f_{l'}\right) = \pm 1$, depending on the number of particles present in the system. For the large systems, that is at the thermodynamic limit, one can neglect these additional terms and solve it exactly [103].

In the remaining part of this chapter, we shall study the HCBs without referring the spinless fermions. Applying Fourier transformations

$$b_l = \frac{1}{\sqrt{L}} \sum_{k\in[-\pi,\pi]} e^{ikl}\, \tilde{b}_k \quad \text{and} \quad b_l^\dagger = \frac{1}{\sqrt{L}} \sum_{k\in[-\pi,\pi]} e^{-ikl}\, \tilde{b}_k^\dagger,$$

where $\tilde{b}_k$ and $\tilde{b}_k^\dagger$ are the bosonic operators in the momentum space. Note that, in the momentum space, the HCBs are just the normal bosons, i.e., $\tilde{b}_k^2 \neq 0$ and $\tilde{b}_k^{\dagger^2} \neq 0$. In the momentum space, the Hamiltonian becomes:

$$H = -\sum_{k\in[-\pi,\pi]} (2\cos k)\, \tilde{b}_k^\dagger \tilde{b}_k. \tag{4.5}$$

The function $\cos k$ is positive in the 1st and 4th quadrants and negative in the other two quadrants. Therefore, we can separate the Brillouin zone $[-\pi, \pi]$ in two sub-Brillouin zones: $[-\frac{\pi}{2}, \frac{\pi}{2}]$ and $[\frac{\pi}{2}, \frac{3\pi}{2}]$. Hence, we can write the above Hamiltonian in

the momentum space also as

$$\begin{aligned} H &= -\sum_{k\in[-\frac{\pi}{2},\frac{\pi}{2}]} \left[(2\cos k)\,\tilde{b}_k^\dagger \tilde{b}_k + 2\cos(k+\pi)\,\tilde{b}_{k+\pi}^\dagger \tilde{b}_{k+\pi}\right] \\ &= -\sum_{k\in[-\frac{\pi}{2},\frac{\pi}{2}]} (2\cos k)\left(\tilde{b}_k^\dagger \tilde{b}_k - \tilde{b}_{k+\pi}^\dagger \tilde{b}_{k+\pi}\right). \end{aligned} \tag{4.6}$$

The above expression can be written more compact way in terms of Nambu's spinor: $\begin{pmatrix} \tilde{b}_k & \tilde{b}_{k+\pi} \end{pmatrix}^T$ as

$$H = -\sum_{k\,\in\,[-\frac{\pi}{2},\frac{\pi}{2}]} \left[\begin{pmatrix} \tilde{b}_k^\dagger & \tilde{b}_{k+\pi}^\dagger \end{pmatrix} (2\cos k)\,\sigma_z \begin{pmatrix} \tilde{b}_k \\ \\ \tilde{b}_{k+\pi} \end{pmatrix} \right]. \tag{4.7}$$

Here the Hamiltonian H is written for the all possible values of k varying from $-\frac{\pi}{2}$ to $\frac{\pi}{2}$. The Hamiltonian for a definite value of k, also known as the Hamiltonian kernel, is:

$$H_k^0 = -(2\cos k)\,\sigma_z, \tag{4.8}$$

where σ_z is a pseudospin operator represented by a Pauli matrix. The periodic boundary condition $b_{L+1} = b_1$ gives $e^{ikL} = 1$, i.e., $k = 2m\pi/L$, where m are integers. The above form of the Hamiltonian indicates that the system has two bands, represented by $|k\rangle$ and $|k+\pi\rangle$, where $-\frac{\pi}{2} \le k \le \frac{\pi}{2}$. For a given k, we can describe these bands as:

$$|k\rangle = \begin{pmatrix} 1 \\ \\ 0 \end{pmatrix},\ |k+\pi\rangle = \begin{pmatrix} 0 \\ \\ 1 \end{pmatrix}. \tag{4.9}$$

For the half-filling case, the band $|k\rangle$ with $-\frac{\pi}{2}$ to $\frac{\pi}{2}$ is filled. The ground state for every k mode is then $(1\ \ 0)^T$, the up state of the pseudospin operator σ_z.

If the system is perturbed by a staggered onsite potential of the form

$$V = -\alpha \sum_{l=1}^{L} (-1)^l \, b_l^\dagger b_l, \tag{4.10}$$

then the two modes with momenta $|k\rangle$ and $|k+\pi\rangle$ will couple. Here, V is expressed in the lattice space. This potential can also be expressed in the momentum space, by the standard Fourier transformation. We replace $(-1)^l = e^{\pm i\pi l}$, and then in the Nambu's spinor representation, we can write the onsite potential in the k-space as:

$$V = \sum_{k\in[-\frac{\pi}{2},\frac{\pi}{2}]} \left[\begin{pmatrix} \tilde{b}_k^\dagger & \tilde{b}_{k+\pi}^\dagger \end{pmatrix} (-\alpha\sigma_x) \begin{pmatrix} \tilde{b}_k \\ \tilde{b}_{k+\pi} \end{pmatrix} \right]. \tag{4.11}$$

Here the kernel corresponding to the potential is

$$V_k = -\alpha\sigma_x. \tag{4.12}$$

Then the kernel of the total Hamiltonian will be

$$H_k = H_k^0 + V_k = -(2\cos k)\sigma_z - \alpha\sigma_x. \tag{4.13}$$

This potential opens up an energy gap at $k = \pm\frac{\pi}{2}$ and system becomes bosonic Mott-insulator (gapped phase) for any nonzero value of α. Therefore, the applied onsite staggered potential introduces a quantum phase transition from the superfluid phase or the gapless phase for $\alpha = 0$, to the Mott insulator phase or the gapped phase for any $\alpha \neq 0$. Here we shall consider this onsite potential as time-dependent $V \to V(t)$, which also leads to $V_k \to V_k(t)$. In addition, we consider this potential as time-periodic, i.e., $V(t+T) = V(t)$ or $V_k(t+T) = V_k(t)$. Then the total Hamiltonian $H_k(t)$ in the momentum space will become time-periodic

having a static part H_k^0 and a time-periodic part $V_k(t)$. Therefore, we can study this system from the Floquet theory perspective.

4.2.2 Driving protocols

In general, we can write the time-periodic onsite staggered potential as

$$V(t) = -\alpha F(t) \sum_{l=1}^{L} (-1)^l b_l^\dagger b_l, \tag{4.14}$$

We have considered two different driving protocols.

1. Single kicked HCBs, i.e., the system experiences the staggered potential in δ-kicked form, only once within a single period:

$$F(t) = \sum_{n=1}^{\infty} \delta(t - nT) \tag{4.15}$$

2. Double kicked HCBs, i.e., the staggered potential acts on the system twice within a single time period in δ-kicked form; and the polarity of the two kicks, separated by a finite time, is opposite:

$$F(t) = \sum_{n=1}^{\infty} \left\{ \delta \left[t - (2n - 1 - \Delta)\frac{T}{2} \right] - \delta \left[t - (2n - 1 + \Delta)\frac{T}{2} \right] \right\}. \tag{4.16}$$

Here, Δ is the time interval between the two kicks. The *negative* sign in between the two δ-functions is indicating the opposite polarity of the two kicks.

4.2.3 Observables: Current and Work done

Current: The current operator is defined in the following way [104, 105]: first we introduce a vector potential $A = \nu/L$ where ν can be considered as a *pseudo*

magnetic flux piercing through the HCB ring of L number of sites. Then the free Hamiltonian becomes

$$H_\nu = -\sum_l \left(b_l^\dagger b_{l+1} e^{-i\nu} \, + \, b_{l+1}^\dagger b_l e^{i\nu} \right). \tag{4.17}$$

The flux ν is also called a boost to the system. Then the current operator will be

$$\widehat{j} = -\frac{1}{L}\left(\frac{\partial H_\nu}{\partial \nu}\right)_{\nu=0} = \frac{i}{L}\sum_{l=1}^{L}\left(b_{l+1}^\dagger b_l \, - \, b_l^\dagger b_{l+1} \right) \tag{4.18}$$

in the lattice space and

$$\widehat{j}_k = \frac{2}{L}\,\sigma_z \,\sin k \tag{4.19}$$

in the momentum space.

Work done: The other observable which we study is the work done $W_d(t)$ on the system by the driving field. For the periodic driving case, after n time period or after the time $t = nT$, the work done in the momentum space will be

$$W_d(nT) = \frac{1}{L}\sum_k \left[e_k(nT) - e_k(0) \right], \tag{4.20}$$

where $e_k(nT) = \langle \Psi_k(nT)|H_k|\Psi_k(nT)\rangle = -2\langle \Psi_k(nT)|\sigma_z|\Psi_k(nT)\rangle \cos k$ is the average energy stored in the system after $t = nT$ and $e_k(0) = \langle \Psi_k(0)|H_k|\Psi_k(0)\rangle = -2\langle \Psi_k(0)|\sigma_z|\Psi_k(0)\rangle \cos k$ is the energy stored in the system before the start of periodic driving.

4.2.4 Initial state

The ground state $|\psi_{0k}\rangle$ of the undriven part of the original Hamiltonian (without boost) carries no current, i.e., $\langle \psi_{0k}|\widehat{j}_k|\psi_{0k}\rangle = 0$. Therefore, we consider the ground state $|\psi_{0k}^{(\nu)}\rangle$ of the boosted Hamiltonian as our initial state. This state has nonzero

current, i.e., $\langle\psi_{0k}^{(\nu)}|\widehat{j}_k|\psi_{0k}^{(\nu)}\rangle \neq 0$. The reason behind this nonzero current is the following: the kernel of the boosted Hamiltonian for each k mode is

$$H_k^{0\nu} = -2\,\sigma_z \cos(k-\nu). \tag{4.21}$$

The Hamiltonian shows that the boost effectively shifts the momentum from k to $k-\nu$. This shifts in the momentum, results in a shift of the ground state. Now the ground state in the range $-\frac{\pi}{2} \leq k \leq -\frac{\pi}{2}+\nu$ is $(0\ \ 1)^T$, which is $|k+\pi\rangle$ mode or band of the un-boosted system. Similarly, the ground state in the range $-\frac{\pi}{2}+\nu \leq k \leq \frac{\pi}{2}$ is $(1\ \ 0)^T$, which is the $|k\rangle$ band of the un-boosted Hamiltonian. For the half-filling case, the $|k\rangle$ band with $[-\frac{\pi}{2}, \frac{\pi}{2}]$ is occupied. After the application of the boost, some part of $|k+\pi\rangle$ band is filled up. This asymmetry in the k space, gives a nonzero current in the ground state of the boosted Hamiltonian. At the thermodynamic limit ($L \to \infty$), this initial nonzero current is: $J_{\text{in}} = \frac{2}{\pi}\sin\nu$. Therefore, we consider this state as the initial state $|\Psi_k(0)\rangle$ for all our subsequent study, i.e.,

$$\begin{aligned} |\Psi_k(0)\rangle &= \begin{pmatrix} 0 \\ 1 \end{pmatrix} \text{ for } -\frac{\pi}{2} \leq k \leq -\frac{\pi}{2}+\nu \\ &= \begin{pmatrix} 1 \\ 0 \end{pmatrix} \text{ for } -\frac{\pi}{2}+\nu \leq k \leq \frac{\pi}{2}. \end{aligned} \tag{4.22}$$

We are particularly interested to study the dynamics of this nonzero current carrying ground state of the boosted Hamiltonian of the HCB system by the unboosted Hamiltonian ($\nu = 0$) perturbed by the periodically driven onsite staggered potential with two different above mentioned driving protocols.

For the sake of completeness, we end this subsection with a fact regarding the boost. The transformation $b_l \to e^{i\nu l}b_l$ removes ν from each term of the boosted

Hamiltonian, except the last term, which represents the hopping from the site L to the first site. The phase factor of the last term becomes $e^{i\nu L}$, which is ν-dependent and L is the number of sites. This phase factor can also be interpreted as a *twist* is given to an open HCB chain and then join the two ends of the chain to satisfy the periodic boundary condition.

A complete derivation is presented in C.1.

4.2.5 Dynamics of current and work done

We have set our model, driving protocols, observables to investigate, and also the initial state. We now formulate the dynamics of the two observables. For this, we first need to construct the time evolution operator. From the time-periodic Hamiltonian, we can always construct the time evolution operator for a fixed momentum k within a single time period. This time evolution operator is also known as the Floquet operator. We denote this operator by $\mathcal{F}_k(T)$. In the momentum space, for a given momentum k, the Hamiltonian is written in terms of the Pauli matrices. Therefore, for the kicked drivings, the Floquet operator will be a product of multiple unitary operators and each such operator will be an exponential function of the Pauli matrices. The driving protocol will decide the number of unitary operators in the expression of the Floquet operator. Nevertheless, irrespective of the driving protocol, we can always express the Floquet operator as a single exponential function of the Pauli matrices using a well known identity

$$e^{ia(\vec{\sigma}.\hat{n})}\, e^{ib(\vec{\sigma}.\hat{m})} = e^{ic(\vec{\sigma}.\hat{l})}, \tag{4.23}$$

where $\{a, b, c\}$ are scalars and $\{\hat{n}, \hat{m}, \hat{l}\}$ are unit vectors. Here c and $\hat{l}$ can be found in terms of $a, b, \hat{n}$ and $\hat{m}$ using the following identity:

$$\begin{aligned}\cos c &= \cos a\, \cos b - \hat{n}.\hat{m}\, \sin a\, \sin b \\ \hat{l} &= \frac{1}{\sin c}\big(\hat{n} \sin a\, \cos b + \hat{m}\, \sin b \cos a - \hat{n} \times \hat{m}\, \sin a\, \sin b\big).\end{aligned} \tag{4.24}$$

Therefore, in general, the Floquet operator can always be expressed for the time period T as

$$\mathcal{F}_k(T) = e^{-i\mu_k T(\vec{\sigma}.\hat{l})}, \tag{4.25}$$

where μ_k is the quasienergy of the mode k.

Current: The total particle current flowing through the system for all k-modes is obtained as:

$$J(nT) = \sum_k J_k(nT) = \sum_k \langle \Psi_k(nT)|\widehat{j}_k|\Psi_k(nT)\rangle, \tag{4.26}$$

where $\widehat{j}_k = \frac{2}{L}\sigma_z \sin k$ and $|\Psi_k(nT)\rangle = \mathcal{F}_k(T)^n|\Psi_k(0)\rangle$. We have already fixed the initial state $|\Psi_k(0)\rangle$. We can write the current flow more explicitly as

$$\begin{aligned}J(nT) &= \frac{2}{L}\sum_k \sin k \langle \Psi_k(0)|\mathcal{F}_k(T)^{n\dagger}\sigma_z \mathcal{F}_k(T)^n|\Psi_k(0)\rangle \\ &= \frac{2}{L}\sum_k \Big[\cos^2(\mu_k nT) + (l_z^2 - l_x^2 - l_y^2)\sin^2(\mu_k nT)\Big]\langle \Psi_k(0)|\sigma_z|\Psi_k(0)\rangle\, \sin k,\end{aligned} \tag{4.27}$$

where l_i with $i \in (x, y, z)$ are the components of the unit vector $\hat{l}$ and therefore $l_x^2 + l_y^2 + l_z^2 = 1$. Using this relation, we write the total current at time $t = nT$ as

$$J(nT) = \frac{2}{L}\sum_k f(k)\langle \Psi_k(0)|\sigma_z|\Psi_k(0)\rangle \sin k, \tag{4.28}$$

where $f(k) = [1 - 2(1 - l_z^2)\sin^2(\mu_k nT)]$. At the asymptotic limit $nT \to \infty$, we can replace $\sin^2(\mu_k nT)$ with its average value over one single cycle that is

$\sin^2(\mu_k nT) = 1/2$, therefore we get $f(k) = l_z^2$ and consequently

$$J(\infty) = \frac{2}{L}\sum_k l_z^2 \langle\Psi_k(0)|\sigma_z|\Psi_k(0)\rangle \sin k. \tag{4.29}$$

At the thermodynamics limit $L \to \infty$, we can write $\frac{2\pi}{L}\sum_k \to \int dk$, therefore

$$\begin{aligned} J(\infty) &= \frac{1}{\pi}\int_{-\frac{\pi}{2}}^{\frac{\pi}{2}} l_z^2\langle\Psi_k(0)|\sigma_z|\Psi_k(0)\rangle \sin k\, dk \\ &= \frac{1}{\pi}\Bigg[\int_{-\frac{\pi}{2}}^{-\frac{\pi}{2}+\nu} l_z^2\langle\Psi_k(0)|\sigma_z|\Psi_k(0)\rangle \sin k\, dk \\ &\qquad + \int_{-\frac{\pi}{2}+\nu}^{\frac{\pi}{2}} l_z^2\langle\Psi_k(0)|\sigma_z|\Psi_k(0)\rangle \sin k\, dk\Bigg] \\ &= \frac{1}{\pi}\Bigg[-\int_{-\frac{\pi}{2}}^{-\frac{\pi}{2}+\nu} l_z^2 \sin k\, dk + \int_{-\frac{\pi}{2}+\nu}^{\frac{\pi}{2}} l_z^2 \sin k\, dk\Bigg]. \end{aligned} \tag{4.30}$$

Finally, by substituting $k \to k + \pi$ in the second term of the above expression, we get

$$J(\infty) = -\frac{2}{\pi}\int_{-\frac{\pi}{2}}^{-\frac{\pi}{2}+\nu} l_z^2 \sin k dk. \tag{4.31}$$

The parameter l_z is determined by the driving protocols.

Work done: Following the definition of the work done on the system by the driving, given in Eq. (4.20), and using the undriven Hamiltonian $H_k^0 = (2\cos k)\sigma_z$, we get

$$W_d(nT) = -\frac{2}{L}\sum_k \Big[\langle\Psi_k(nT)|\sigma_z|\Psi_k(nT)\rangle \; - \; \langle\Psi_k(0)|\sigma_z|\Psi_k(0)\rangle\Big] \cos k. \tag{4.32}$$

At the asymptotic limit $nT \to \infty$, we get

$$W_d(\infty) = -\frac{2}{L}\sum_k (l_z^2 - 1)\langle\Psi_k(0)|\sigma_z|\Psi_k(0)\rangle. \cos k, \tag{4.33}$$

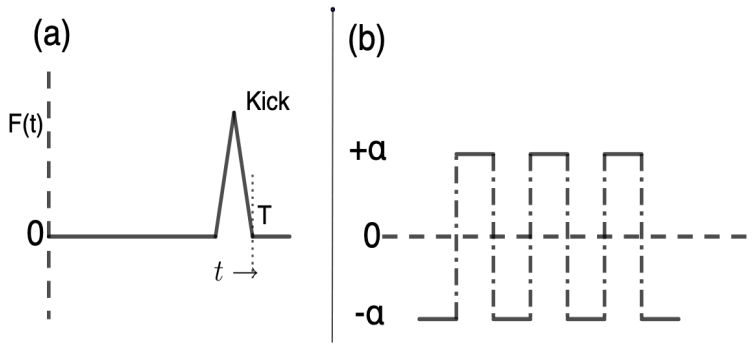

FIGURE 4.1: (a) The driving scheme is shown within the time period $[0, T]$. This driving scheme will repeat itself in every period T. (b) Shape of the staggered potential is shown at the time of kick at $t = nT$.

At the thermodynamics limit, $L \to \infty$, the above expression becomes

$$\begin{aligned} W_d(\infty) &= -\frac{1}{\pi}\int_{-\frac{\pi}{2}}^{\frac{\pi}{2}} (l_z^2 - 1)\langle\Psi_k(0)|\sigma_z|\Psi_k(0)\rangle \cos k \\ &= \frac{2}{\pi}\cos\nu - \frac{1}{\pi}\int_{-\frac{\pi}{2}+\nu}^{\frac{\pi}{2}+\nu} l_z^2 \cos k\, dk. \end{aligned} \tag{4.34}$$

Here, l_z is the same parameter as defined earlier.

4.3 Single kick hard core bosons (SKHCB)

Figure 4.1 has diagrammatically presented the driving protocol. The Hamiltonian kernel for the single kick HCBs in the momentum space $(k,\, k+\pi)$ is:

$$H_k(t) = -2\,\sigma_z\,\cos k - \alpha\,\sigma_x F(t) \quad \text{where} \quad F(t) = \sum_{n=1}^{\infty}\delta(t - nT). \tag{4.35}$$

The Floquet operator is obtained from the relation $\mathcal{F}_k(T) = \mathcal{T}e^{-i\int_0^T H_k(t)dt}$, where $\mathcal{T}$ is denoting the time ordering, as:

$$\mathcal{F}_k(T) = e^{i2\sigma_z \cos kT}\, e^{i\alpha\sigma_x} = e^{-iH_{\text{eff}}T}. \tag{4.36}$$

Unlike any generic case, here we can determine the effective Hamiltonian analytically exact and obtain the form $H_{\text{eff}} = \mu_k \vec{\sigma}.\hat{l}$. Using the identities given in Eqs. (4.23) and (4.24), the quasienergies μ_k is obtained as

$$\mu_k = \pm\frac{1}{T}\cos^{-1}\left[\cos(2\cos kT)\cos\alpha\right] \tag{4.37}$$

and the components of the unit vector $\hat{l}$ as

$$\begin{aligned} l_x &= \frac{\cos(2T\cos k)\sin\alpha}{\sin(\mu_k T)} \\ l_y &= -\frac{\sin(2T\cos k)\sin\alpha}{\sin(\mu_k T)} \\ l_z &= \frac{\sin(2T\cos k)\cos\alpha}{\sin(\mu_k T)}. \end{aligned} \tag{4.38}$$

At the large frequency limit $\omega \to \infty$ or the small time period limit $T \to 0$, we get approximately $l_z^2 = \frac{16\pi^2}{\omega^2}\cot^2\alpha\cos^2 k$. The asymptotic current, derived in Eq. (4.31), at the high frequency limit gives a fixed saturation current J_{sat}. Substituting the approximate l_z in Eq. (4.31), we get

$$J_{\text{sat}} = \frac{32\pi}{3\omega^2}\cot^2\alpha\,\sin^3\nu. \tag{4.39}$$

Similar way, from Eq. (4.34), we obtain the saturated work done as

$$W_{\text{sat}} = \frac{2}{\pi}\cos\nu. \tag{4.40}$$

The same relation of the saturation current and work done were obtained earlier in Ref. [40] but by different means.

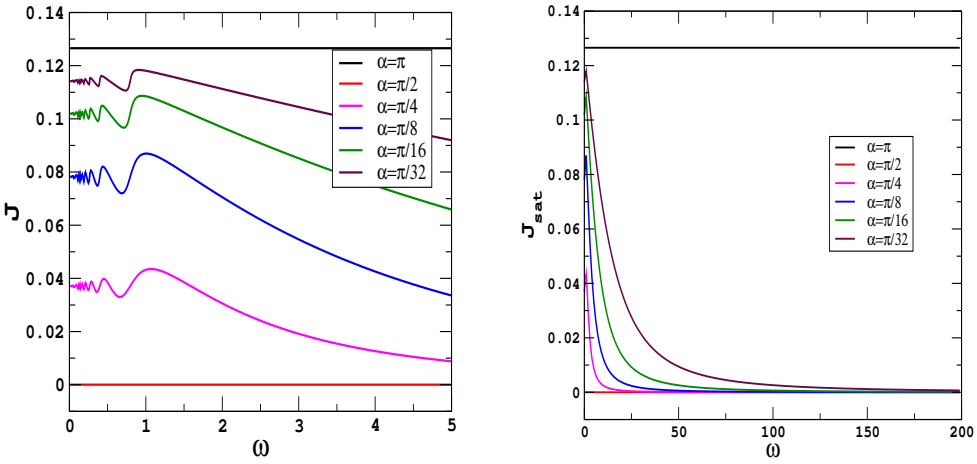

FIGURE 4.2: (a) In left panel current is plotted as a function of driving frequency ω (small) for different α for fix twist $\nu = 0.2$. (b) In right panel current is investigated as a function of driving frequency ω at a large limit for different kicking strength α for fix value of twist $\nu = 0.2$

4.3.1 Some more results of current

We investigate the current and work done as a function of the driving frequency ω, for different values of kicking strength α. In Fig. 4.2, the total current for single kicked HCBs system is investigated as a function of the periodic driving frequency ω. The left panel of the figure shows that, except for two cases of kick strength $\alpha = \frac{\pi}{2}$ and π, the current shows dips and peaks at smaller values of ω for all other kicking strength α. For higher values of ω, the current decays asymptotically. This indicates the presence of *dynamical localization* in the system. For $\alpha = \frac{\pi}{2}$, the Floquet operator becomes

$$\mathcal{F}_k(T, \alpha = \frac{\pi}{2}) = \sigma_x \exp(i2T \cos k\, \sigma_z).$$

Since the initial state is an eigenstate of σ_z, the second term of $\mathcal{F}_k(T, \alpha = \frac{\pi}{2})$ will only introduce a global phase factor to the initial state and then σ_x flips the state to the other eigenstate of σ_z and thus the current will immediately become *zero*

and remain fixed at that value with time evolution. For the other case $\alpha = \pi$,

$$\mathcal{F}_k(T, \alpha = \pi) = \exp(i2T \cos k\, \sigma_z).$$

Again, the reason just mentioned above, this operator will introduce only a global phase to the initial state and thus the current will remain fix at the initial value.

At the right panel, the saturation current J_{sat} is studied as a function of ω. For $\alpha = \pi$, due to the same reason stated above, the saturation current is also remained fixed at the initial current. Again, as we discussed just above, the saturation current also remains fixed at 0 for $\alpha = \frac{\pi}{2}$ and shows dynamical localization for all values of driving strength α. For small values of ν, the saturation current becomes

$$J \to \frac{32\pi}{3}\nu^3 \frac{\cot^2 \alpha}{\omega^2}, \tag{4.41}$$

which is known as ν^3 law [106].

4.3.2 Some more results of work done

We have also investigated the work done on the system by the driving as a function of the frequency ω. The left panel of Fig. 4.3 shows that the work done on the system also shows dips and peaks for smaller values of driving frequency. However, this dips and peaks are at different values of ω as observed in case of the current. Actually, the current and the work done shows anticorrelation. This is an expected result because when the current flow through the system drops, one has to do more work to maintain the flow. The opposite thing happens when the current flow is high. The right panel of Fig. 4.3 shows that, for larger values of ω, the work done reaches a finite saturation value which agrees with our analytically calculated J_{sat}

.

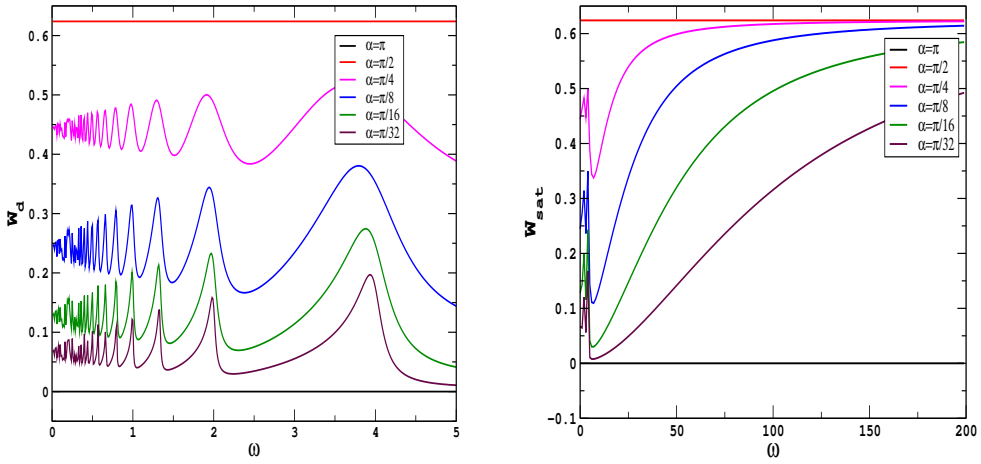

FIGURE 4.3: Left panel of figure shows work done on the system as a function of driving frequency ω (small) for different kicking strength α for fix twist $\nu = 0.2$ and right panel shows the investigation of work done as a function of driving strength ω for large values for different kicking strength α with fix $\nu = 0.2$.

From these studies, we conclude that the HCBs system in the presence of periodic single δ-function kicked driving shows dynamical localization at the high frequency limit. These results agree well with a previous study which used different method to obtain these results [40].

4.4 Double kick hard core bosons (DKHCB)

At the left column of Fig. 4.4, we have shown the pair of δ-kicks by a diagram. Two kicks act on the system symmetrically about the time $\frac{T}{2}$ at $t = T_{\mp} = (1 \mp \Delta)\frac{T}{2}$. Here the two kicks are of opposite polarities. At the right column of the figure, we have shown the onsite staggered potential at the time of each kick.

The Floquet operator for the double kicked case is:

$$\begin{aligned} \mathcal{F}_k(T) = &\exp[iT(1-\Delta)\sigma_z \cos k] \exp[i\alpha\sigma_x] \exp[i2T\Delta\sigma_z \cos k] \\ &\exp[-i\alpha\sigma_x] \exp[iT(1-\Delta)\sigma_z \cos k] = \exp(-iH_{\text{eff}}T), \end{aligned} \tag{4.42}$$

where the effective Hamiltonian also has the form of $H_{\text{eff}} = \mu_k \vec{\sigma}.\hat{l}$. The above

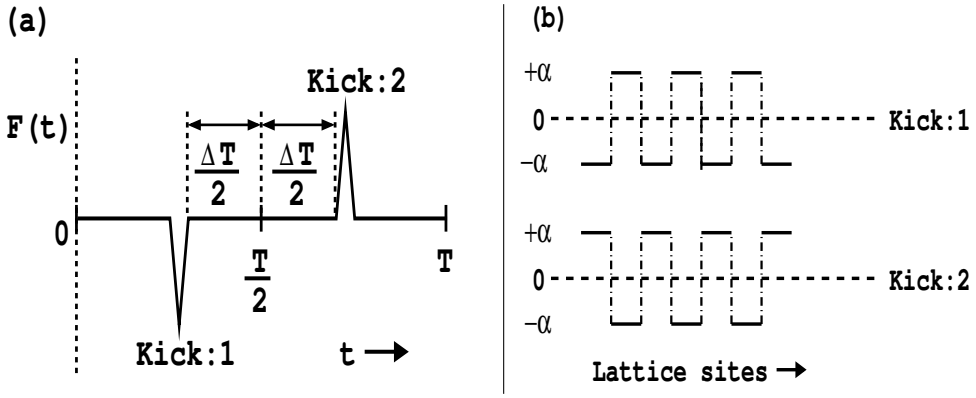

FIGURE 4.4: (a) The driving scheme is shown within the time period $[0, T]$. This driving scheme will repeat itself in between any arbitrary interval of nT and $(n+1)T$. (b) The shape of the staggered potentials are shown at the time of two kicks (at $t_{\mp} = \frac{1}{2}(1 \mp \Delta)T$).

expression shows that the Floquet operator is a product of *five* unitary operators. Therefore, we have to apply the identity given in Eq. (4.23) multiple times to get H_{eff}. Then following Eq. (4.24), we get

$$\mu_k^{\pm} = \pm\frac{1}{T}\cos^{-1}\Big[\cos^2\alpha\cos(2T\cos k) + \sin^2\alpha\cos(2T(1-2\Delta)\cos k)\Big] \tag{4.43}$$

and

$$\begin{aligned} l_x &= 0, \\ l_y &= \frac{\sin(2\alpha)\sin(2T\Delta\cos k)}{[1-\{\cos^2\alpha\cos(2T\cos k) + \sin^2\alpha\cos(2T(1-2\Delta)\cos k)\}^2]^{1/2}}, \end{aligned} \tag{4.44}$$

and

$$l_z = \frac{\cos^2\alpha\sin(2T\cos k) + \sin^2\alpha\sin(2T(1-2\Delta)\cos k)}{[1-\{\cos^2\alpha\cos(2T\cos k) + \sin^2\alpha\cos(2T(1-2\Delta)\cos k)\}^2]^{1/2}}.$$

For a complete derivation, see C.4.

From the expression of the Floquet operator Eq. (4.42) and (4.44), one can easily observe that for some specific values of $\alpha = \pm m\pi, \pm(2m+1)\frac{\pi}{2}$, where $m = 0, 1, 2, ..$, the time evolving state remains frozen at its initial state. From Eq. (4.44), we see that at these values of α, the component $l_y = 0$ and $l_z = 1.0$. This suggest

that the effective Hamiltonian becomes proportional to σ_z and hence the initial state will not evolve under the operation of $\mathcal{F}_k(T)$. Therefore, the current flow remains fixed at its initial value. The Floquet operator for $\alpha = 0$ and $\alpha = \pi$ are identical. Naturally, all the physical properties are expected to be the same at these two values of α. Consequently, the Floquet operator itself and all the physical properties repeat themselves within every interval $m\pi \leq \alpha \leq (m+1)\pi, m \in \mathbb{Z}$. Hence, it is sufficient to consider α within 0 to π. Interestingly, at $\alpha = \frac{\pi}{2}$ the corresponding Floquet operator $\mathcal{F}_k$ become the Hermitian conjugate of the Floquet operator corresponding to $\alpha = 0$ or π. If α is replaced by $\alpha + \frac{\pi}{2}$ where $\alpha < \frac{\pi}{2}$, then the Floquet operator $\mathcal{F}_k(T)$ transforms in to its Hermitian conjugate, i.e $\mathcal{F}_k(T) \rightarrow \mathcal{F}_k^{\dagger}(T)$. This suggests that if we investigate any local observable as a function of α, then that observable should show a mirror symmetry about $\alpha = \frac{\pi}{2}$. Later, we see that this is indeed the case and the local observables like the current flow through the system and the work done on the system follow this symmetry property.

Initially, a boost ν is applied to the system of hard core bosons (HCB) to induce a nonzero current (superfluid state), and then the boost is withdrawn. After that, the system is evolved under the time evolution operator $\mathcal{F}_k(T)$ from the initial current carrying state. The hard core bosonic ring remains in the superfluid state except at the time of two δ-function kicks. The staggered potential is applied at the time of each kick that creates a gap in the energy band which indicates a phase transition in the system and the system becomes a bosonic Mott insulator. As a result, the current flow remains fixed to its initial value without any drop during the free motion, and the system momentarily becomes Mott insulator at the time of each kick which leads to a drop in the current flow. Here we are interested to investigate the effect of the periodically kicked staggered onsite potential on the

initial current flow. In a recent study, a complete disappearance of current flow at the asymptotic limit and also at the large frequency limit is shown under the presence of single δ-function kick [40]. Here we are interested to investigate the current flow and work done in the system of hard core bosons (HCB) under the double δ-functions kick driving protocol.

At the asymptotic limit $nT \to \infty$, using Eq. (4.29), we get

$$\begin{aligned} J(\infty) &= \frac{2}{L}\sum_k {l_z}^2 \langle\Psi_k(0)|\sigma_z|\Psi_k(0)\rangle \sin k \\ &= \frac{2}{L}\sum_k \left[\frac{\cos^2\alpha \sin(2T\cos k) + \sin^2\alpha \sin(2T(1-2\Delta)\cos k)}{\left[1-\{\cos^2\alpha\cos(2T\cos k)+\sin^2\alpha\cos(2T(1-2\Delta)\cos k)\}^2\right]^{1/2}}\right]^2 \\ &\langle\Psi_k(0)|\sigma_z|\Psi_k(0)\rangle \sin k. \end{aligned} \tag{4.45}$$

From the above, we also like to estimate the *saturation current* defines as $J_{\rm sat} \equiv \lim_{\omega\to\infty}\lim_{nT\to\infty} J(nT)$. For the saturation current $J_{\rm sat}$, the limit $\omega \to \infty$ implies $T \to 0$, therefore we have chosen the limit $n \to \infty$ in such a manner that time nT also approaches towards ∞. Thus we get,

$$J_{\rm sat} = \frac{2}{L}\left[\frac{\cos^2\alpha + (1-2\Delta)\sin^2\alpha}{\sqrt{\cos^2\alpha + (1-2\Delta)^2\sin^2\alpha}}\right]^2 \sum_k \langle\Psi_k(0)|\sigma_z|\Psi_k(0)\rangle \sin k. \tag{4.46}$$

Here l_z is independent of k. We know that at the thermodynamics limit $L \to \infty$, one can replace $2\pi/L\sum_k \to \int dk$ as:

$$\begin{aligned} J_{\rm sat} &= \frac{1}{\pi} l_z^2 \int_{-\frac{\pi}{2}}^{\frac{\pi}{2}} \langle\Psi_k(0)|\sigma_z|\Psi_k(0)\rangle \sin k\, dk \\ &= \frac{l_z^2}{\pi}\left[\int_{-\frac{\pi}{2}}^{-\frac{\pi}{2}+\nu} \langle\Psi_k(0)|\sigma_z|\Psi_k(0)\rangle \sin k\, dk + \int_{-\frac{\pi}{2}+\nu}^{\frac{\pi}{2}} \langle\Psi_k(0)|\sigma_z|\Psi_k(0)\rangle \sin k\right] \\ &= \frac{2\, l_z^2 \sin\nu}{\pi} = l_z^2\, J_{\rm in}. \end{aligned} \tag{4.47}$$

Unlike the SKHCB case, the above expression suggests that the saturation current is independent of the driving frequency ω. This expression is valid for all values of α and Δ, except when concurrently $\alpha = \frac{\pi}{2}$ and $\Delta = 0.5$. For these values, l_z becomes indeterminate of the form $(0/0)$. It is observed that, for $\alpha = \frac{\pi}{2}$, the Floquet time evolution operator becomes $e^{i2T(1-2\Delta)\sigma_z \cos k} = e^{-i(1-2\Delta)H_k T}$. Therefore we get $H_{\text{eff}} = (1-2\Delta)H_k = -2(1-2\Delta)\sigma_z \cos k$. As a result $\mu_k = (1-2\Delta)\cos k$ and $l_z = 1$. Now, if the parameter, $\Delta = 0.5$, effective Hamiltonian becomes a *null* operator and the time evolution operator becomes $\mathcal{F}_k = \mathbb{1}$, where $\mathbb{1}$ is the identity operator. Therefore, any dynamics with time evolution is absent for this case and the initial state remains as it is. As a consequence, the current flow in the system remains fixed at its initial value, which can be obtained by substituting $l_z^2 = 1$, as:

$$J(nT) = \frac{1}{\pi}\int_{-\frac{\pi}{2}}^{\frac{\pi}{2}} dk f(k)\langle\psi_k(0)|\sigma_z|\psi_k(0)\rangle = \frac{2}{\pi}\sin\nu = J_{\text{in}}. \tag{4.48}$$

For other values of driving strength α, current flow through the system drops and therefore some work is needed to be done on the system to maintain the steady flow of current.

We have also studied another local observable, that is the work done on the system. The work done measures the amount of energy absorbed by the system from the external driving. In the same spirit, as we define the saturation current, the *saturated work done* is defined as $W_{\text{sat}} \equiv \lim_{\omega\to\infty}\lim_{nT\to\infty} W_d(nT)$. At the thermodynamics limit $L \to \infty$ we obtain a simple expression for saturated work done on the system as:

$$W_{\text{sat}} = \frac{1}{\pi}(1-l_z^2)\cos\nu. \tag{4.49}$$

The presence of the factor l_z^2 in the expression of the current and $(1-l_z^2)$ in the work done, gives a clear indication that these two observables are anticorrelated.

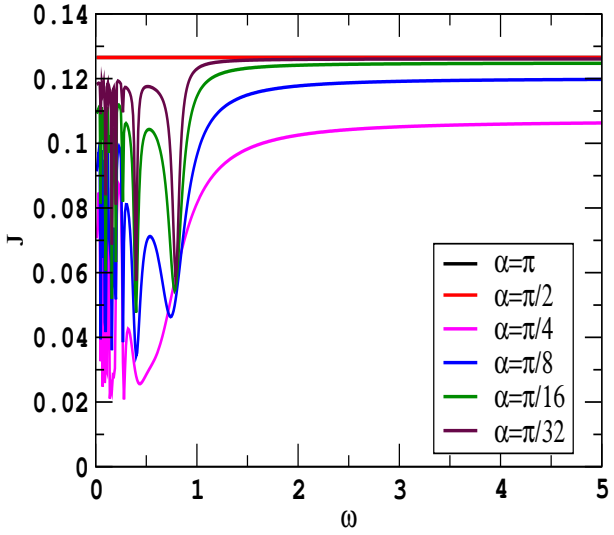

FIGURE 4.5: The asymptotic current versus the driving frequency ω is plotted for different values of driving strength α. Here we set $\Delta = 0.3$ and the initial current is set by applying a twist $\nu = 0.2$. Here we see that the current is saturation at different finite values at large ω limit, but we do not see any DL.

4.4.1 Some more results of the current flow

We now present some more results of the current flow. We have studied this as a function of the driving frequency ω, driving strength α, time interval between the two kicks Δ, and the initial current determined by the initial boost ν.

The asymptotic current versus the driving frequency ω:

In Fig. 4.5, the asymptotic current is investigated as a function of the driving frequency ω for different kicking strengths α and a fixed $\Delta = 0.3$. The parameter Δ is the time interval between the two kicks. Here, for the smaller values of ω, the current flow through the system shows *peaks and dips*. However, for large values of ω, the current flow reaches to a saturation value irrespective of the kicking strength α. Since, we have already derived that $J_{\rm sat}$ is independent of driving frequency ω for the double kicked case, we do not expect to see a complete decay of saturation current at the large frequency limit. We now discuss elaborately the behavior of the current flow for different driving strengths.

Figure 4.5 shows that, if $\alpha = \frac{\pi}{2}$ and π, the current remains fixed at its initial value. For $\alpha = \frac{\pi}{2}$, the effective Hamiltonian becomes $H_{\text{eff}} = (1 - 2\Delta)H_k$. Here, for $\Delta = 0.3$, the effective Hamiltonian is proportional to the free Hamiltonian H_k. For $\alpha = \pi$, the time evolution Floquet operator becomes $\mathcal{F}_k = e^{i2T\sigma_z \cos k} = e^{-iH_kT}$, i.e., $H_{\text{eff}} = H_k$. We know that initial state $|\psi(0)\rangle$ is the ground state of the twisted Hamiltonian H_k^ν, which is also an eigenstate of σ_z. Therefore, $|\psi(0)\rangle$ is a stationary state for the time evolution operator when $\alpha = \frac{\pi}{2}$ and π, and thus for these values of α the current remains fixed at its initial value 0.1265 for any Δ.

We have also plotted the asymptotic current for other values of α. It is found that, for $\alpha = \frac{\pi}{4}, \frac{\pi}{8}$, and $\frac{\pi}{16}$, the current shows again such dips and peaks for smaller values of driving frequency when $\omega < 1$, and then it reaches to some finite saturation value as ω increases. The saturation values satisfy very accurately with our analytical estimation. Following the reason discussed above, the maximum value of the saturation current is observed for $\alpha = \frac{\pi}{2}$ and $\alpha = \pi$. On the other hand, the minimum value is obtained at $\alpha = \frac{\pi}{4}$ but that never reaches to *zero*. Hence, in the DKHCB system, the current survives at the asymptotic limit, which indicates absence of dynamical localization (DL). Here the current is calculated both analytically and numerically, and they agrees very well. Figure 4.5 shows that the asymptotic current saturates around $\omega = 5$. Therefore, for all practical purpose, $\omega > 5$ can be considered as sufficiently large. We now study the saturation current as a function of different parameters.

The saturation current versus the kicking strength α:

In Fig. 4.6, the saturation current is investigated as a function of the kicking strength α for different values of Δ with a fixed twist $\nu = 0.2$. Here it is observed that, for all values of Δ, the saturation current varies periodically as a function of α. Each curve shows mirror symmetry about $\alpha = \frac{\pi}{2}$, i.e., J_{sat} is equal at α

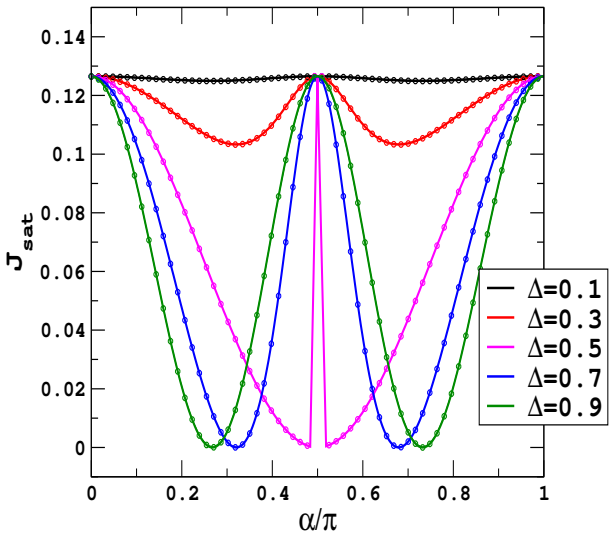

FIGURE 4.6: The saturation current J_{sat} is plotted as a function of α for different values of the parameter Δ. Solid lines are the exact numerical results and the solid circles are representing our analytical estimation.

and $\pi - \alpha$. It is also clear from this figure that, for $\alpha = 0, \frac{\pi}{2}$ and π, the saturation current remains fixed at its initial value. Here solid lines show the exact results and solid circles show analytical estimation. We see a very good agreement between them.

Here we do not see any disappearance of current for any driving strength α for $\Delta < 0.5$. The condition $J_{\text{sat}} = 0$ can be estimated by setting $l_z = 0$. The expression of l_z shows that it is not possible to find a real value of α to satisfy this condition when $\Delta < 0.5$. For $\Delta = 0.5$, the saturation current decreases with increasing α. It attains the maximum value sharply at the neighbourhood $\alpha \lesssim \frac{\pi}{2}$ and then again drops sharply when $\alpha \gtrsim \frac{\pi}{2}$. After that it smoothly increases and reaches to the maximum value at $\alpha = \pi$. At $\Delta = 0.5$, $l_z = \cos\alpha$ and $J_{\text{sat}} = J_{\text{in}} \cos^2\alpha$. Therefore, as we increases the kicking strength α, the saturation current J_{sat} decreases and become almost negligible for $\alpha \lesssim \frac{\pi}{2}$. But at $\alpha = \frac{\pi}{2}$, there is a discontinuity in J_{sat}. This we discussed earlier that, at this value of α, the driving term becomes $\mathbb{1}$, and therefore we get $l_z = 1$ and thus $J_{\text{sat}} = J_{\text{in}}$. Further, when $\alpha \gtrsim \frac{\pi}{2}$, the saturation current J_{sat} again start increasing from a very small value to attain its initial value

$J_{\text{sat}} = J_{\text{in}}$ at $\alpha = \pi$.

Within the range $0.5 < \Delta \leq 1$, we observe complete disappearances of J_{sat} at some values of α less than $\frac{\pi}{2}$ and also at $\pi - \alpha$ due to the symmetry discussed earlier. We determine this value of α by setting $l_z = 0$, and that gives the condition:

$$\begin{aligned} \cot^2 \alpha &= \sqrt{2\Delta - 1}, \\ \text{and hence } \alpha &= \pm \cot^{-1}(\sqrt{2\Delta - 1}) \\ &= \cot^{-1}(\sqrt{2\Delta - 1}) \text{ and } \pi - \cot^{-1}(\sqrt{2\Delta - 1}). \end{aligned} \tag{4.50}$$

According to the above condition, the saturation current J_{sat} disappears for $\Delta = 0.7$ when $\alpha = \pm \cot^{-1}(\sqrt{.04}) \simeq 1.007$ and 2.135. Similarly, the saturation current disappears at $\alpha \simeq 0.841$ and 2.301 for $\Delta = 0.9$. Fig. 4.6 confirms these results.

The saturation current versus the time interval between two kicks Δ:

From the expression of the current, we see that besides the driving strength α, the current can also be tuned with the parameter Δ. We now study how the saturation current can be tuned by varying Δ. In Fig. 4.7, this result is shown by investigating the saturation current as a function of Δ. First, a trivial point is to be noted that, at $\Delta = 0$, the saturation current for all values of α is the same, which can be easily understood from Fig. 4.4. This figure clearly shows that, when $\Delta = 0$, both the kicks act at the same time and then their opposite polarity cancels each other. That means the dynamics of the system is governed by the free Hamiltonian only and hence the effective Hamiltonian $H_{\text{eff}} = H_k = -2\sigma_z \cos k$. Therefore, due to the absence of δ-kicks, the initial current carrying ground state $|\psi(0)\rangle$ remains stationary under the time evolution and consequently the current flow in the system remains fixed at the initial value $J_{\text{in}} = \frac{2}{\pi} \sin \nu \simeq 0.126$ irrespective of the driving strength α.

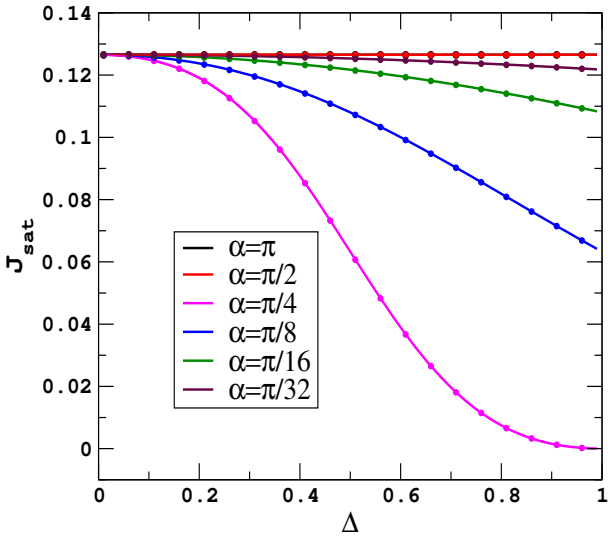

FIGURE 4.7: The saturation current J_{sat} is plotted as a function of the time interval between two kicks determined by the parameter Δ, for different values of the kicking strength α. Solid lines are representing exact numerical calculation, whereas the circles are representing our analytical estimation.

Here again, the saturation current for $\alpha = \frac{\pi}{2}$ and $\alpha = \pi$ are the same and remain constant at the initial value, as observed in Fig. 4.5. For other values of α, the saturation current shows decay with the increasing Δ. For $\alpha = \frac{\pi}{4}$, the saturation current J_{sat} reaches to 0 when Δ approaches to *unity*. At $\Delta = 1$ the dynamics is very much different which we see from the expression of the Floquet operator as:

$$\mathcal{F}_k(T) = \exp(i\alpha\sigma_x)\, \exp[i\, 2T\sigma_z \cos k]\, \exp(-i\alpha\sigma_x). \tag{4.51}$$

Therefore, after a time interval $t = nT$, the time evolution operator will be

$$\mathcal{F}_k(nT) = \mathcal{F}_k(T)^n = \exp(i\alpha\sigma_x)\, \exp[i2nT\sigma_z \cos k]\, \exp(-i\alpha\sigma_x). \tag{4.52}$$

This suggests that, at $\Delta = 1$, in addition to an initial and a final kick, the dynamics is governed by the free Hamiltonian $H_k = 2\sigma_z \cos k$ for the whole time interval $t = nT$. As a result the dynamics of the system at $\Delta = 1$ is fundamentally different from the double-kicked system. Hence, here we ignore this particular case

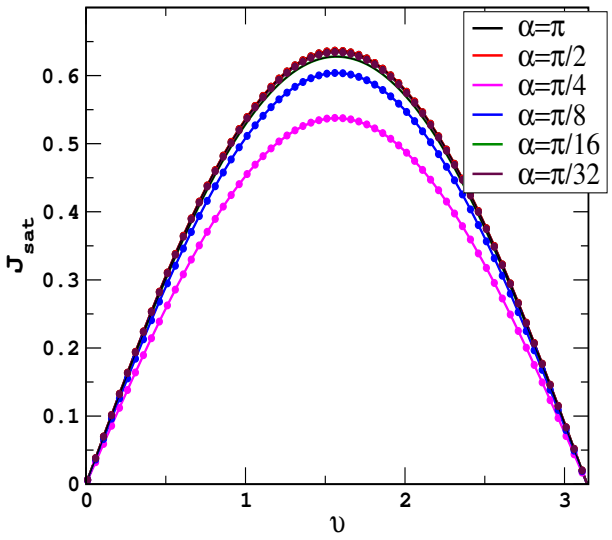

FIGURE 4.8: The saturation current $J_{\rm sat}$ is plotted as a function of the initial boost ν. As we discussed in the text, here $J_{\rm sat} \propto \sin\nu$. This suggests that, unlike the observed "ν^3-law" in case of the singled kicked HCB system, here the double kicked HCB system follows $J_{\rm sat} \propto \nu$ at very small twist $\nu \ll 1$.

and all the results are shown for $\Delta < 0.9$. For other values of α, the saturation current does not reach close to zero for $\Delta \lesssim 1$. In Fig. 4.7, solid lines show the exact numerical results and the circles show the analytically calculated results, and they are in very good agreement.

The saturation current as a function of the initial current via ν:

Finally, we are interested to investigate the saturation current $J_{\rm sat}$ as a function of the initial current $J_{\rm in}$, via the parameter ν. Therefore, in Fig. 4.8, instead of plotting the saturation current as a function of the initial current, we have presented exact numerics together with the analytical estimation for the saturation current as a function of the initial twist for different values of kicking strength α, at a fixed parameter $\Delta = 0.3$.

Figure 4.8, shows that the saturation current increases with the increment of ν and reaches maxima when $\nu = \frac{\pi}{2}$. This is expected because, when we increase the initial twist, the overlap between the two bands $|k\rangle$ and $|k+\pi\rangle$ increases and that

leads to the increment in the initial current. It is very logical that the saturation current should also increase with the increment in the initial current. However, for further increase of the twist when $\nu > \frac{\pi}{2}$, the overlap between the two bands decreases and consequently initial current also decreases. Again, that leads to the drop in the saturation current. We have already found that $J_{\text{sat}} \propto \sin\nu$. This suggests that, for very small values of twist $\nu \ll 1$, we have $J_{\text{sat}} \propto \nu$. This behavior is fundamentally different from the single kicked case, where $J_{\text{sat}} \propto \nu^3$. Here again the exact numerical results and our analytically estimation agree well.

4.4.2 Some more results of the work done

We have seen that the HCB system driven with an onsite staggered potential is responsible for the drops in the current. In order to maintain the current flow through the system one has to do some work on the system and consequently the system stores some energy which is also known as the residual energy [107]. Here again, we have studied the work done on the system as a function of the driving frequency ω, driving strength α, time interval between the two kicks Δ, and the initial current determined by the boost ν.

The work done on the system versus the driving frequency ω:

In Fig. 4.9, the work done on the system is investigated as a function of the driving frequency ω for different kicking strengths α. Here, we fix the parameters $\Delta = 0.3$ and $\nu = 0.2$. From the figure, we can see that for $\alpha = \frac{\pi}{2}$ and $\alpha = \pi$ the work done on the system is *zero*. This result was expected as we observed in Fig. 4.5 that the current remain constant at its initial value for these two driving cases and therefore no work to be done to maintain the current flow.

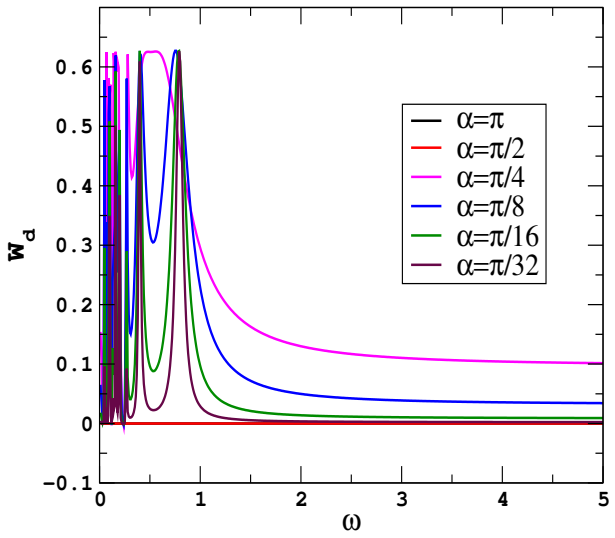

FIGURE 4.9: The asymptotic work done $W(\infty)$ is plotted as a function of ω for different values of the driving strength α. Here we set the values of the other parameters same as given in Figure 4.5

For the other values of the driving strength α, the periodically kicked staggered potential introduces a gap in the system at the time of each kick and that leads to a drop in the current flow in the system. Therefore, some work is to be done on the system to maintain the current flow. Hence, for these cases, the work done also shows peaks and dips up to $\omega = 1$, and for $\omega > 1$ work done on the system reaches to some finite value. However, according to the expectation, we observe an anticorrelation between the peaks and dips of the asymptotic current $J(\infty)$ and the asymptotic work done $W_d(\infty)$, i.e., whenever $J(\infty)$ shows a peak, then $W_d(\infty)$ shows a dip exactly at the same value of ω and vice versa. For $\omega > 1$, the work done starts to saturate and reaches to its saturation value around $\omega \gtrsim 5$. This behavior of the work done is consistent with the current flow result. Here, the saturation of the work done suggests that the system reaches a steady state and stops absorbing any energy from the driving [108]. The exact numerical results (solid lines) and the analytical estimation (solid circles) are in good agreements.

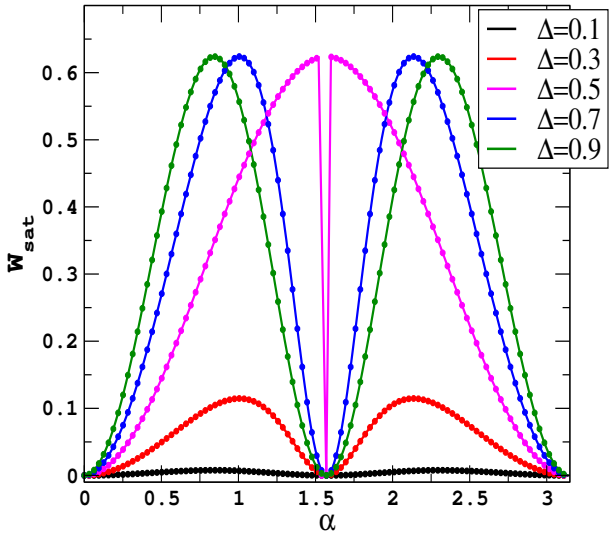

FIGURE 4.10: The saturated work done W_{sat} versus the driving strength α is plotted for different values of Δ. The initial boost is $\nu = 0.2$. Solid lines and the circles are respectively representing the exact numerical calculation and the analytical estimation.

The saturated work done versus the kicking strength α:

In Fig. 4.10, the work done is investigated as a function of the kicking strength α for different Δ and a fixed twist $\nu = 0.2$. The work done shows a sinusoidal behavior with the variation of α. As we increase Δ, the saturated work done also increases. This is because more work is needed to be done on the system to maintain the steady current flow. At $\alpha = 0$, π and $\frac{\pi}{2}$, the results are same for all values of Δ. For these cases, the current flow remains fixed at its initial value, and therefore no work is to be done to maintain the current flow. If we compare Figs. 4.6 and 4.10, then we notice that lower values of J_{sat} demands higher value of W_{sat} and vice versa. This anticorrelation has already been explained. Again the exact numerics and the analytical estimation are in good agreements.

The saturated work done versus the time interval between two kicks Δ:

In Fig. 4.11, the saturated work done is presented as a function of Δ for different kicking strengths α and a fixed $\nu = 0.2$. Initially, when $\Delta = 0$, the two kicks

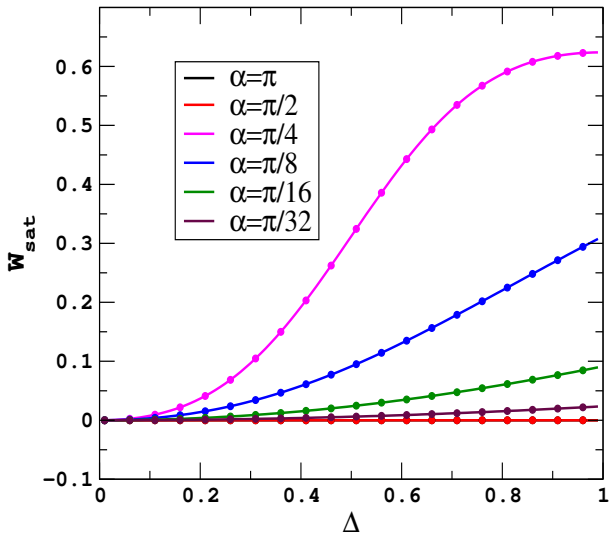

FIGURE 4.11: The saturated work done $W_{\rm sat}$ is plotted as a function of the parameter Δ which determines the time interval between two kicks for different values of the driving strength α. The initial twist $\nu = 0.2$. Solid lines and the circles are respectively representing the exact numerical calculation and the analytical estimation.

are acting at the same time in the opposite direction and thus cancel each other. Therefore, the current remain fixed at its initial value and consequently the saturated work done is also remain fixed at zero. As we increase Δ, the current flow shows drop from its initial value. Then work has to be done on the system to maintain the current flow. Therefore, the saturated work done $W_{\rm sat}$ increases with Δ. However, again $\alpha = \frac{\pi}{2}$ and π are two special cases where the saturated work done remains fixed at zero. The saturated work done reaches the maximum value for the kicking strength $\alpha = \frac{\pi}{4}$. For other values of $\alpha < \frac{\pi}{4}$, the maximum possible value of the saturated work done is less.

The results of Fig. 4.11 are according to our expectations: (i) whenever the saturation current $J_{\rm sat} = J_{\rm in}$, the saturated work done on the system $W_{\rm sat} = 0$, and (ii) whenever the saturation current drops from its initial value the saturated work done becomes nonzero whether that drop is due to the variation of the driving strength α or the variation of the parameter Δ.

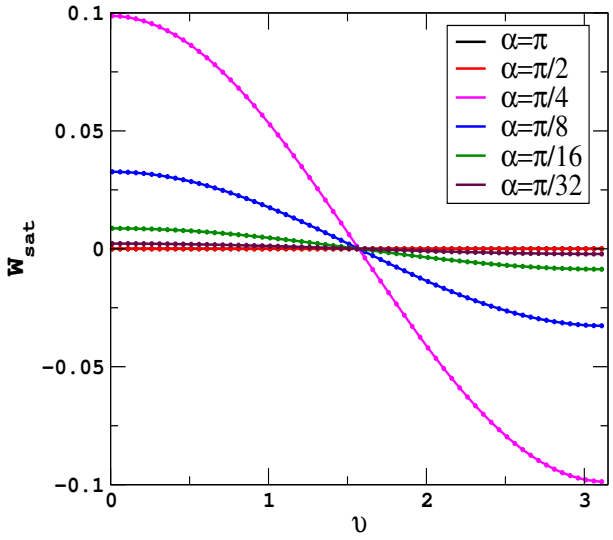

FIGURE 4.12: The saturated work done is plotted as a function of the applied boost/twist ν for different kicking strength α.

The saturated work done versus the initial boost/twist ν:

In Fig. 4.12, the work done is investigated as a function of the twist ν for different values of kicking strength α and a fixed $\Delta = 0.3$. Here, as usual, the saturated work done for $\alpha = \frac{\pi}{2}$ and π is zero. An interesting property which we see here that W_{sat} is becoming negative for $\nu > \frac{\pi}{2}$. For these cases, the twist can be considered as given in the opposite direction and that reverses the direction of the current. Therefore, in order to maintain the current flow along the reverse direction, one has to do work in the opposite direction and hence the saturated work done shows negative values.

4.4.3 Time evolution of density of particles

In Fig 4.13, the dynamics of the density of particles is investigated on the lattice. The time is plotted stroboscopically along the x-axis and the location of the lattice sites l are presented along y-axis. A system of 200 lattice sites is considered. The panels of Fig.4.13 show the particles at the lattice sites as a function of the stroboscopic time $t = nT$ for different time period T and the driving strength α.

Here, we are interested for the kicking strength $\alpha = \frac{\pi}{2}$. Initially, at $n = 0$, one particle is kept at each site from 50 to 150 and the other sites are kept empty. This initial state is represented by a diagonal density matrix $\rho(0)$ of dimension 200. Its 51st to 150th diagonal elements are equal to *one* and all the remaining elements are *zero*. Here, the trace of the density matrix is equal to the number of particles, that is 100 here. The ratio of the number of particles and the number of sites is 1/2. As we mentioned earlier, here we are considering the half-filled case. The evolution of the density matrix is obtained from $\rho(nT) = \mathcal{F}_k(nT)\rho(0)\mathcal{F}_k^\dagger(nT)$, where $\rho(0)$ is the initial density matrix and $\mathcal{F}_k(nT)$ is the time evolution operator for the DKHCB system.

As $t = nT$ increases, the particles are expected to spread with maximum velocity determined by the absolute value of the group velocity $v_k^\pm$, defined as $v_k^\pm = \frac{d\mu_k^\pm}{dk}$. The group velocity can be obtained from the quasi-energies following the given relation. At kicking strength $\alpha = \frac{\pi}{2}$, the quasienergy is defined as:

$$\mu_k^\pm = \pm 2(1 - 2\Delta)\, \cos k, \tag{4.53}$$

and from this we get

$$v_k^\pm = \frac{d\mu_k^\pm}{dk} = \mp 2(1 - 2\Delta) \sin k. \tag{4.54}$$

The maxima of the absolute value of group velocity is obtained by substituting maximum value of $\sin k$, i.e $\sin k = 1$. This gives $|v_k^\pm| = 2(1 - 2\Delta)$. Here we consider, $\Delta \leq 0.5$. We are not interested to discuss the results for $\Delta \geq 0.5$ because quasienergy has symmetry about $\Delta = 0.5$ i.e, Δ and $(1 - \Delta)$ gives the same quasienergy $\mu_k^\pm$.

We observe the spreading of the particle stroboscopically and found that the boundary separating the occupied and unoccupied regions are spreading linearly in

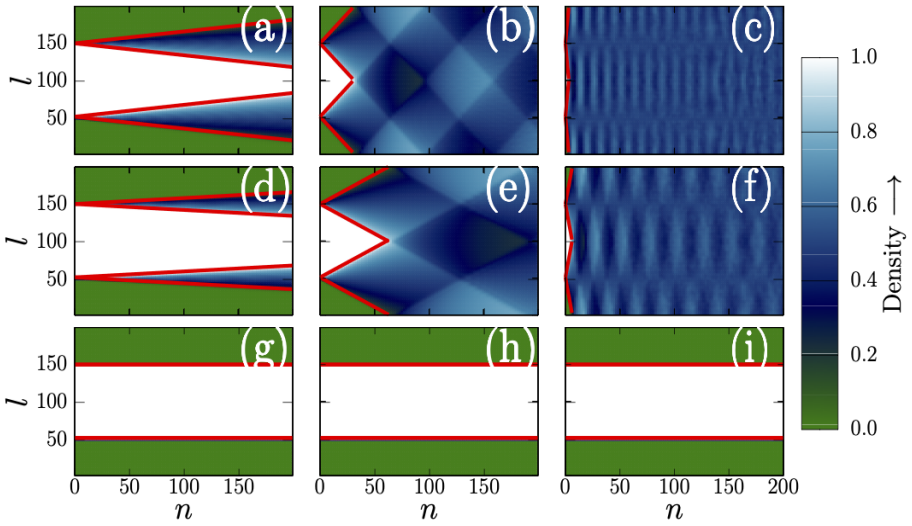

FIGURE 4.13: The time-evolutions of the density of particles placed in a HCB system of 200 lattice sites are shown as a function of the stroboscopic time $t = nT$ for a fixed value $\alpha = \frac{\pi}{2}$. Here, as we go from the left to the right, the time period T varies; and when we go from the top to the bottom, the parameter Δ varies: (a) $\Delta = 0.1$, $T = 0.1$; (b) $\Delta = 0.1$, $T = 1.0$; (c) $\Delta = 0.1$, $T = 10.0$; (d) $\Delta = 0.3$, $T = 0.1$; (e) $\Delta = 0.3$, $T = 1.0$; (f) $\Delta = 0.3$, $T = 10.0$; (g) $\Delta = 0.5$, $T = 0.1$; (h) $\Delta = 0.5$, $T = 1.0$; and (i) $\Delta = 0.5$, $T = 10.0$. Solid red lines are showing the boundaries of the light-cone like regions.

light-cone like fashion with a rate determined by $\max|v_k^{\pm}|$. Therefore, the equation for this dynamics of the linear spreading in the configuration space or lattice space can be written as:

$$\frac{dl}{dt} = \frac{1}{T}\frac{dl}{dn} = \pm \max|v_k^{\pm}| = \pm 2(1-2\Delta). \tag{4.55}$$

For the spreading of particles, the slope is given by the maximum value of $|v_k^{\pm}|$ as a function of k. For a particle initially placed at some lattice point l_0, where $51 \leq l_0 \leq 150$; then at any arbitrary instant n, the particle will be at site l, where $l = l_0 \pm 2(1-2\Delta)nT$.

In Figs. 4.13(a)-(c), the red colored solid lines are showing the linear spreading of the boundaries. These boundaries are obtained from the evolution of the particles place initially at site 51 and 150. In Fig. 4.13(a), the time period is 0.1 and

$\Delta = 0.1$. Here we observe that these particles have reached the boundaries of the lattice at $l = 200$ very slowly. In Figs. 4.13(b) and 4.9(c), for larger values of T, the particles reach the boundaries very fast. Qualitatively similar behavior is observed for $\Delta = 0.3$ and the results are presented in Figs. 4.13(d)-(f).

In Figs. 4.13(g)-(i), we have shown the results for $\Delta = 0.5$. For this value of Δ, particle remains to its initial lattice site l_0 for all n and T. This is because, for $\Delta = 0.5$ together with $\alpha = \frac{\pi}{2}$, the effective Hamiltonian becomes a *null* operator. Therefore, there will not be any dynamical evolution. Consequently, all the particles will remain fixed at its initial positions $51 \leq l_0 \leq 150$ unless there is any initial current. These figures looks similar to the dynamical localization in the density profile dynamics in the SKHCB system, but here the origin of this localization is due to a very trivial reason, i.e. absence of any dynamics.

We are presenting the results for $\alpha = \frac{\pi}{2}$ only, because the dynamical behavior of the density of particles will qualitatively remain the same for any other values of α. This means that, for any values of Δ, the $v_k^{\pm} \neq 0$ and thus the density of particles will evolve in light-cone like fashion. The light-cone like spreading has been studied theoretically [109] and also realized experimentally following a quantum quench [110].

4.4.4 Phase Diagram

From our extensive study of the current flow through the system and the work done on the system of HCBs, we conclude that the parameter l_z^2 is the most important one, which determines the dynamics of the system. That is understandable from the relation $J_{\text{sat}} \propto l_z^2$ and $W_{\text{sat}} \propto (1 - l_z^2)$. The current flow, as well as the work done on the system, is dependent on whether the system is in superfluid phase or Mott insulator phase or intermediate of the both. Therefore, the parameter

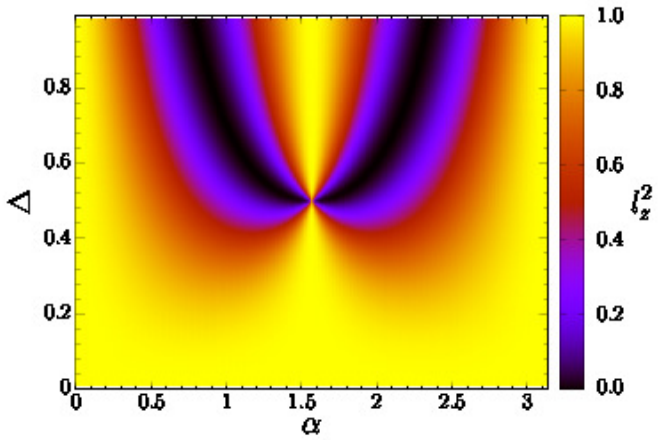

FIGURE 4.14: The phase diagram of the system is presented by a density plot of the parameter l_z^2 as a function of the parameters α and Δ. This figure shows the system can be in three major phases: (i) Yellow region: Superfluid phase; (ii) Black region: bosonic Mott insulator phase; (iii) Red and Violet: Intermediate of superfluid and insulator phase.

l_z^2 determines the phase of the system. The parameter l_z^2 can be tuned by two parameters: (i) kicking strength α and (ii) time interval between the two kicks Δ. In Fig. 4.14, we show the phase diagram of the system by a density plot of l_z^2 as a function of the parameter α and Δ.

In previous results, we have considered only certain values of α and Δ to study the current flow through the system and work done on the system. Here in the phase diagram, we can now see an overall picture of different phases of the system. Figure 4.14 reveals that a major part of the phase diagram is covered by the yellow colored region, where $l_z^2 = 1$. This region is representing the superfluid phase.

On the other hand, we see a much smaller black region in the upper half part ($\Delta \geq 0.5$) of the diagram where $l_z^2 = 0$. In this parameter regime, the periodic driving has completely destroyed the superfluid property and the system has become a Mott insulator. This behavior can also be attributed to the dynamical localization. A careful observation reveals that the insulator region is separated into two parts at ($\alpha = \frac{\pi}{2}$, $\Delta = 0.5$). At this particular point of the phase diagram, the parameter

l_z^2 is again equaled to *unity* and the system becomes superfluid.

Besides these two extreme regions where $l_z^2 = 1.0$ and $l_z^2 = 0$, in the remaining part of the phase diagram l_z^2 is fraction. In the red region, l_z^2 is slightly less than 1.0. This indicates a marginal current drop in the system. That means, the system is behaving very much like superfluid but having a small effect of the bosonic Mott insulating phase due to the driving. However, the scenario becomes opposite in the violet region. Here, the insulating phase is dominating and the superfluid contribution is very small. This leads to a larger drop in the current, but we do not observe complete disappearance of the current due to the dynamical localization. One may say that, in red and violet regions, the system shows a partial dynamical localization.

4.5 Conclusion

We have studied a chain of hard core bosonic system with periodic boundary condition experiencing a periodically driven onsite staggered potential. We have considered following driving protocols: (1) a single δ-kick within the time period T; and (2) double δ-kicks separated by a finite time interval within T, where the polarity of the two kicks are opposite. The single kicked HCB system has been studied recently, so we have focussed mostly on the double kicked case. However, for the sake of completeness, we have applied our formalism to study some properties of the single kicked system and found good agreement with the results presented in an earlier work.

We have mostly studied two observables: the current flow through the system and the work done on the system by the periodic driving. For the single kicked case, as reported earlier also, we have observed a dynamical localization which results in to the complete decay of the initial current. For the double kicked case, we

have studied these two observables as a function of the driving frequency, driving strength, interval between the two kicks, and also initial current. The general observation is that the current flow and the work done are anticorrelated. This means that, whenever due to the driving, the initial current through the system drops, we need to do work on the system to maintain the flow of the current. We can think of two extreme cases. First, when the current flow does not drop from its value, we do not have to do any work on the system and therefore the work done is equal to *zero*. The other one is the situation when the current drops sharply from its initial value to *zero*, and for this case the work done on the system is maximum.

We have also studied the dynamics of the density of particles for the half-filled case. The time evolution of the particle density evolves linearly in light-cone like fashion and the maximum speed of the particles is determined by the absolute value of the group velocity, which is determined from the quasienergies. Finally, we have presented the phase diagram of this dynamics. We have found that, at the periodic steady states, the system can be in three different phases: pure superfluid, pure Mott insulator, and intermediate of these two phases. However, the Mott insulator phase has covered the least amount of the area in the phase diagram and the superfluid phase has occupied most of the region. The latter is happening because, for a major part of the parameter regime, the second kick somehow nullifying the effect of the first kick and preventing the system to become dynamically localized.